

High Affinity Anti-inorganic Material Antibody Generation by Integrating Graft and Evolution Technologies

POTENTIAL OF ANTIBODIES AS BIOINTERFACE MOLECULES*[§]

Received for publication, May 12, 2009, and in revised form, December 23, 2009. Published, JBC Papers in Press, December 31, 2009, DOI 10.1074/jbc.M109.020156

Takamitsu Hattori[‡], Mitsuo Umetsu^{‡§1}, Takeshi Nakanishi[‡], Takanari Togashi[¶], Nozomi Yokoo[¶], Hiroya Abe^{||}, Satoshi Ohara^{||}, Tadafumi Adschiri[¶], and Izumi Kumagai^{‡2}

From the [‡]Department of Biomolecular Engineering, Graduate School of Engineering, Tohoku University, Sendai 980-8579, the [§]Center for Interdisciplinary Research, Tohoku University, Sendai 980-8578, the [¶]Institute of Multidisciplinary Research for Advanced Materials, Tohoku University, Sendai 980-8577, and the ^{||}Joining and Welding Research Institute, Osaka University, Osaka 567-0047, Japan

Recent advances in molecular evolution technology enabled us to identify peptides and antibodies with affinity for inorganic materials. In the field of nanotechnology, the use of the functional peptides and antibodies should aid the construction of interface molecules designed to spontaneously link different nanomaterials; however, few material-binding antibodies, which have much higher affinity than short peptides, have been identified. Here, we generated high affinity antibodies from material-binding peptides by integrating peptide-grafting and phage-display techniques. A material-binding peptide sequence was first grafted into an appropriate loop of the complementarity determining region (CDR) of a camel-type single variable antibody fragment to create a low affinity material-binding antibody. Application of a combinatorial library approach to another CDR loop in the low affinity antibody then clearly and steadily promoted affinity for a specific material surface. Thermodynamic analysis demonstrated that the enthalpy synergistic effect from grafted and selected CDR loops drastically increased the affinity for material surface, indicating the potential of antibody scaffold for creating high affinity small interface units. We show the availability of the construction of antibodies by integrating graft and evolution technology for various inorganic materials and the potential of high affinity material-binding antibodies in biointerface applications.

Peptides and proteins recognize the interfacial surfaces of their corresponding molecules with high affinity and selectivity because of the multiple-point interactions of hydrogen bonds and salt bridges and the surficial complementarities at the inter-

faces. Surface recognition by proteins has also been observed in biopolymers in biological systems (1, 2). Furthermore, the use of recent combinatorial library approaches has enabled the identification of short peptides with affinity for nonbiological inorganic materials (3–5). Peptides that bind materials such as metals, metal oxides, and semiconductors have been identified, and they are expected to be useful in bottom-up fabrication procedures in the field of bio-nanotechnology, such as patterning and assembly of proteins and nanomaterials (6–8), biofunctionalization of nanoparticles (9, 10), and synthesis of crystalline nanometer-sized metal particles (11, 12).

Besides short peptides, antibodies are becoming attractive as novel material-binding molecules because they have higher affinities and specificities than peptides. Antibodies are recognition molecules with high binding affinity and specificity in the immune system, and they have been used widely in the fields of medical and analytical chemistry (13). By the use of general methodologies with *in vivo* immune system and *in vitro* combinatorial selection technologies, antibodies to the surfaces of organic crystals of 1,4-dinitrobenzene (14) and tripeptide (15), magnetite (16), gallium arsenide (17), gold (18), and polyhydroxybutyrate (19) have been identified in immunized mice or in libraries of naturally occurring human antibodies. These results demonstrate the potential of antibodies for recognizing the solid surfaces of bulk materials. However, far fewer material-binding antibodies have been obtained than peptides, because the immunogenic potential of solid materials is not high and the vertebrate immune system is not strongly sensitized by such materials. Even if *in vitro* selection methods are used, the limited library diversity and the strong nonspecific interactions of coat proteins on phages with solid bulk surfaces make selecting positive antibodies difficult.

Here, we generated high affinity antibodies against zinc oxide (ZnO), aluminum oxide (Al₂O₃), and cobalt oxide (CoO) material surfaces by the integration of peptide-grafting and evolutionary technologies (Fig. 1). We first grafted a peptide sequence with affinity for the surface of an inorganic material into a CDR³ loop of the single variable domain of the heavy chain of a heavy

* This work was supported by a scientific research grant from the Ministry of Education, Science, Sports and Culture of Japan (to M. U. and I. K.), the Industrial Technology Research Grant Program 2005 of the New Energy and Industrial Technology Development Organization of Japan (to M. U.), proposal-oriented research promotion program of Japan Science and Technology of Japan (to M. U.), Japan Society for the Promotion of Science research fellowships for young scientists (to T. H.), and in part by The Hosokawa Foundation (to M. U.).

[§] The on-line version of this article (available at <http://www.jbc.org>) contains supplemental Tables S1–S5 and Fig. S1.

¹ To whom correspondence may be addressed: Aoba 6-6-11-608; Aoba-ku, Sendai 980-8579, Japan. Tel.: 81-22-795-7276; Fax: 81-22-795-7276; E-mail: mitsuo@kuma.che.tohoku.ac.jp.

² To whom correspondence may be addressed: Aoba 6-6-11-606, Aoba-ku, Sendai 980-8579, Japan. Tel.: 81-22-795-7274; Fax: 81-22-795-6164; E-mail: kmiz@kuma.che.tohoku.ac.jp.

³ The abbreviations used are: CDR, complementarity determining region; Fv, variable fragment of antibody; GdnHCl, guanidine hydrochloride; VHh, variable domain of heavy chain of heavy chain antibody; ZnOBP, ZnO-binding peptide; sZnOBP, selected ZnO-binding peptide; GFP, green fluorescent protein.

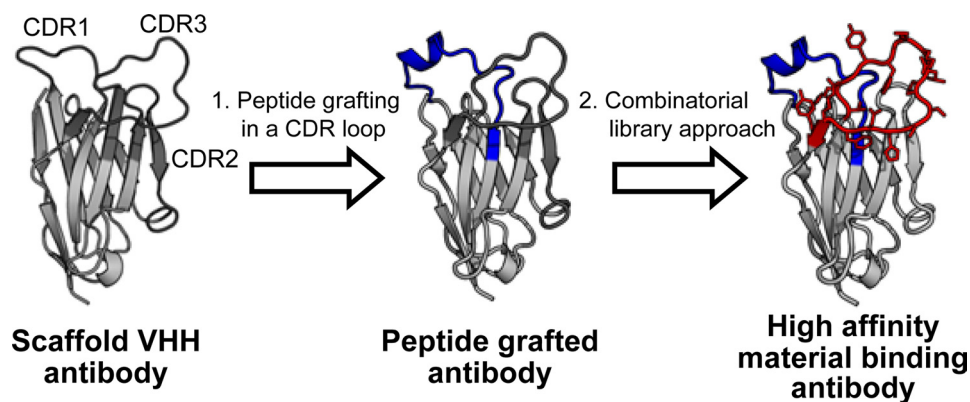


FIGURE 1. Construction of antibody by integrating grafting and evolutionary technologies.

chain camel antibody (VHH) to give a VHH fragment with the same affinity as the grafted peptide and without structural instability. Next, a nonrelated CDR loop in the peptide-grafted VHH was randomized by using an $\alpha\beta\beta\alpha$ motif sequence (see under “Results”) to screen for high affinity antibodies. Application of the single-domain VHH fragment as a framework prevented destabilization in the grafting of the alien peptide in the first step, and construction of a VHH library from the peptide-grafted VHH fragment by using the $\alpha\beta\beta\alpha$ motif sequence enabled us to bypass limitations on library diversity. We also demonstrate the enthalpy synergistic effect from grafted and selected CDR loops on the binding mechanism of antibodies onto material surfaces and the potential of antibody scaffold for creating high affinity small interface units.

EXPERIMENTAL PROCEDURES

Construction of Expression Vectors for VHH Fragment with Material-binding Peptide in CDRs—The DNA sequences coding the VHH fragments of camel anti-BcII β -lactamase antibody cAbBCII10 (20) were synthesized from five oligonucleotides and external primers (supplemental Table S1) by means of overlap extension PCR with LA-Taq DNA polymerase (21). The gene fragments produced were inserted into the NcoI-SacII site of pRA-FLAG vectors containing a FLAG peptide sequence, as constructed previously (22), to produce plasmids for the cAbBCII10 VHH fragment with a FLAG sequence at the C terminus (pRA-wtVHH-FLAG).

The DNA sequences coding the VHH fragment where the CDR loops were replaced with ZnO-, Al₂O₃-, or CoO-binding peptides (11, 23, 24) were generated by means of overlap extension PCR from plasmid pRA-wtVHH-FLAG, using the oligonucleotides and external primers shown in supplemental Table S2. The amplified sequences for the VHH fragments were inserted into the NcoI-SacII sites of the pRA-FLAG vectors to produce the pRA-VHH-FLAG plasmids. For the VHH with a material-binding peptide at the N terminus, the DNA sequences were amplified from the pRA-wtVHH-FLAG plasmid by using the primers in supplemental Table S2 and then inserted into the NcoI-SacII fragment of the pRA-FLAG vector.

Construction of VHH Phage Library and Selection of VHH with High Affinity for Material Surfaces—DNA sequences encoding the VHH_{ZnOBP1}, VHH_{AlOBP1}, and VHH_{CoOBP1} fragments with randomized sequences in the CDR 3 loop were gen-

erated and amplified from the pRA-VHH-FLAG plasmids with each peptide-grafted VHH by using the primers in supplemental Table S3 and overlap extension PCR. The amplified sequences for VHH were inserted into the NcoI-SacII fragment of the phagemid vector of pTZ-PsFv2, which was constructed for phage display of the HyHEL-10 variable fragment (25), to display the VHH fragments on the filamentous bacteriophage M13. For the selection of VHH with high affinity for inorganic materials,

$\sim 10^9$ phages were mixed with 0.2 mg of material particles about 100 nm in diameter (ZnO, Hosokawa Micron Inc., Hirakata, Japan), 200 nm in diameter (Al₂O₃, Taimei Chemicals Co., Ltd., Nagano, Japan), and 40 nm in diameter (CoO, C.I. Kasei Co., Ltd., Tokyo, Japan) in a 10 mM phosphate solution, pH 7.5, with 200 mM NaCl and 0.05% Tween 20 at room temperature for 1 h. The particles were then washed with 10 mM phosphate buffer to remove unbound phages. The residual phages bound to the particles were separated with 200 or 500 mM phosphate solution (200 mM for ZnO and 500 mM for CoO and Al₂O₃), and then the eluted phages were amplified in *Escherichia coli* JM 109 as described previously (25). This panning procedure was performed a total of four times, with increases in the phosphate concentration of the washing solution to 30–50 mM to select the phages displaying antibodies with high affinity for target material surface. After four rounds of selection, the amino acid sequences of the VHH displayed on the isolated phage were analyzed in 200 randomly isolated phage clones. Selected VHH genes were inserted into the NcoI-SacII fragment in the pRA-FLAG vector to express the encoding VHH fragments in *E. coli*.

Using one of the selected VHH genes (4F2 clone), we further prepared the DNA sequences of the selected VHH fragment with CDR 1 loop exchanged for that of cAbBCII10 to evaluate the role of the CDR 3 sequence in selected VHH. The sequences coding the VHH fragment with CDR 1 of cAbBCII10 and CDR 3 of 4F2 VHH were generated by means of overlap extension PCR from plasmid pRA-FLAG vector with the 4F2 VHH gene, using the two oligonucleotides and external primers shown in supplemental Table S4, and the amplified sequences for the VHH fragments were inserted into the NcoI-SacII sites of the pRA-FLAG vectors to produce the pRA-VHH_{sZnOBP3}-FLAG plasmids.

Expression and Purification of VHH Fragments—Transformed *E. coli* BL21 (DE3) cells harboring the expression plasmid encoding VHH fragments were incubated in lysogeny broth medium at 28 °C, and expression of antibody fragments under the control of the T7 promoter was induced by adding 1 mM isopropyl β -D-thiogalactopyranoside. VHH fragments were extracted from the periplasm of the harvested cells by osmotic shock and purified by anion/cation exchange and gel filtration chromatographies after ammonium sulfate treatment.

High Affinity Anti-inorganic Material Antibody Generation

Analysis of Binding Affinities of Antibody Fragments to Material Surfaces—Material particles (0.2 mg) with a Brunauer-Emmett-Teller (BET) specific surface area (surface area estimated by nitrogen gas adsorption (26)) of 9.7 m²/g (ZnO), 12.4 m²/g (Al₂O₃), 30.9 m²/g (CoO), 33.9 m²/g (Fe₂O₃, C. I. Kasei Co., Ltd., Tokyo, Japan), 39.1 m²/g (TiO₂, C. I. Kasei Co., Ltd., Tokyo, Japan), or 39.8 m²/g (NiO, C. I. Kasei Co., Ltd.) were separately added to 300 μl of 10 mM phosphate solution (pH 7.5; 200 mM NaCl, 0.05% Tween 20) containing VHH, and the mixture was incubated for 30 min at several temperatures. After centrifugation at 20,000 × *g* for 10 min, the precipitated particles were added to 300 μl of 6 M guanidine hydrochloride (GdnHCl) solution (10 mM phosphate, 200 mM NaCl, pH 7.5) to elute the adsorbed proteins from the particles. The supernatants were analyzed by SDS-PAGE, and the proteins eluted were quantified with a MicroBCA protein assay reagent kit (Pierce).

Competitive Inhibition Assay for the Binding of VHH onto ZnO with ZnO-binding Peptides—ZnO particles (0.2 mg) were added to 300 μl of a 10 mM phosphate solution containing 3 μM VHH (pH 7.5; 200 mM NaCl, 0.05% Tween 20), and the mixture was incubated for 30 min at 4 °C. After centrifugation at 20,000 × *g* for 10 min, the precipitated ZnO particles were washed with 10 mM phosphate solution to remove nonspecifically adsorbed VHH. After removing the washing solution, the particles were suspended in 300 μl of 10 mM phosphate solutions containing the ZnO-binding peptides at 3 μM, and the suspension was centrifuged at 20,000 × *g* for 10 min. This inhibition procedure was repeated until the concentration of peptides was increased to 3 mM, and all the supernatants were analyzed by SDS-PAGE. Residual VHH on ZnO particle even after the inhibition procedure with 3 mM peptides were eluted with 6 M GdnHCl solution, and the supernatant was also analyzed by SDS-PAGE.

Construction of Bispecific VHH Dimers with Affinity for ZnO Surface and GFP—The sequence of anti-GFP VHH (cAbGFP4) (27) was generated from five oligonucleotides and two external primers (supplemental Table S5) by means of overlap extension PCR with LA-Taq DNA polymerase, and the gene fragments were inserted into the NcoI-SacII site of the pRA-FLAG vectors to produce the plasmids (pRA-cAbGFP4-FLAG). To generate bispecific antibody with affinity for ZnO and GFP, the gene sequence of cAbGFP4 was fused at the C terminus of 4F2 VHH via a llama IgG2 upper hinge-linker (EPKIPQPQPKPQPQPKPQPQPKPQP) (28). The gene sequence was generated and amplified from the plasmids of pRA-4F2VHH-FLAG and pRA-cAbGFP4-FLAG by using the primers in supplemental Table S5, and the amplified gene fragments were inserted into the NcoI-SacII fragment of the pRA-FLAG vector (4F2 VHH-llama IgG2 upper hinge linker-cAbGFP4). The bispecific VHH dimers were expressed in *E. coli* and prepared as for the other VHH fragments.

Reflectometric Interference Spectroscopy—A biosensor array system with reflectometric interference spectroscopy (Fluidware Technology Inc., Kawaguchi, Japan) was used to measure the binding of VHH fragments to ZnO films and the bispecificity of VHH dimers. VHH monomer or bispecific VHH dimer (1 μM) in 10 mM phosphate buffer (pH 7.5; 200 mM NaCl) was

TABLE 1
Amino acid sequences of CDR loops of ZnOBP-grafted VHH fragments

ZnO-binding peptide is underlined. Numbering of the amino acids of cAbBCII10 VHH follows the Kabat numbering system (20). Amino acids of ZnOBP-grafted VHH are numbered as 1–1 to 1–18 (CDR 1 in VHH_{ZnOBP1}), 2–1 to 2–20 (CDR 2 in VHH_{ZnOBP2}), and 3–1 to 3–16 (CDR 3 in VHH_{ZnOBP3}).

Fragment	Sequence of CDR 1	Sequence of CDR 2	Sequence of CDR 3
cAbBCII10	26 35c GGSEYS-YSTFSLG	50 65 95 ATASM--GGLTYADSVK-G	102 VRGYFMRLPSSHNFY
VHH _{ZnOBP1}	1-1 1-18 GGSE <u>EAHVMHKVAPR</u> PSL	50 65 95 ATASM--GGLTYADSVK-G	102 VRGYFMRLPSSHNFY
VHH _{ZnOBP2}	26 35c GGSEYS-YSTFSLG	2-1 2-20 A <u>IAEAHVMHKVAPR</u> PDSVK-G	95 102 VRGYFMRLPSSHNFY
VHH _{ZnOBP3}	26 35c GGSEYS-YSTFSLG	50 65 3-1 ATASM--GGLTYADSVK-G	3-16 <u>VEAHVMHKVAPR</u> PFY

directly flowed for 240 s onto a ZnO film deposited on a silicon plate at the flow rate of 10 μl/min, and the change in wavelength with minimum reflection intensity was measured. For bispecific VHH dimers, 1 μM GFP was further injected after washing with 10 mM phosphate buffer for 240 s.

RESULTS

Design for Grafting ZnO-binding Peptide Sequences into CDR Loops of VHH Fragments—As a scaffold for the VHH fragment, we used the camel anti-BcII β-lactamase antibody cAbBCII10, which has an appropriate framework for CDR replacements (20). Table 1 shows the CDR amino acid sequences of VHH with ZnO-binding peptide (ZnOBP; EAHVMHKVAPRP) (11) in CDR 1 (VHH_{ZnOBP1}), CDR 2 (VHH_{ZnOBP2}), and CDR 3 (VHH_{ZnOBP3}). For grafting of ZnOBP into each CDR, we drew upon the crystal structure of the chimera of cAbBCII10 where the CDRs were replaced with those of cAbLys3 (20). In the crystal structure, the N-terminal side of CDR 2 and the C-terminal sides of CDRs 1 and 3 form β structures with the adjacent framework sequences; this has been observed in most reported VHH structures (29, 30). We preserved the edge sequences of the CDRs when the CDR loops were replaced with the ZnOBP sequence.

The crystal structure of ungrafted cAbBCII10 VHH was reported recently (31). It resembles that of the chimeric cAbBCII10; consequently, we confirmed that our grafting design suited the crystal structure of ungrafted cAbBCII10 VHH.

Structure and Binding Ability of VHH Fragments with ZnO-binding Peptide Sequence Grafted in Their CDR Loops—All the ZnOBP-grafted VHH fragments were expressed as soluble forms in *E. coli*, although the VHH_{ZnOBP2} fragments were expressed mainly as insoluble aggregates (data not shown). Analysis of VHH_{ZnOBP1} and VHH_{ZnOBP3} by size-exclusion chromatography and examination of circular dichroism spectra demonstrated a monomeric form with the typical immunoglobulin structure of camel antibody (Fig. 2). However, VHH_{ZnOBP2} formed oligomers with a random structure. Grafting of the peptide sequences into CDR 1 or CDR 3 resulted in little structural change in the framework, but grafting into CDR 2 led to deformation of the camel-type immunoglobulin structure. Reports of the conformational structures of VHH indicate

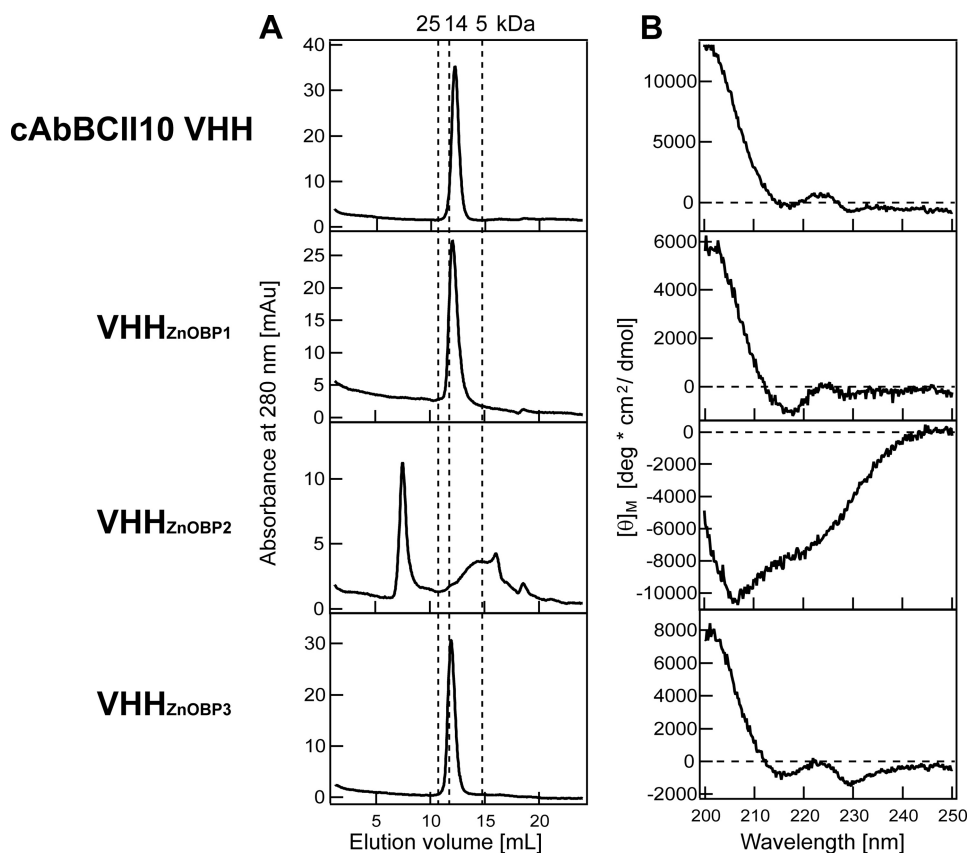


FIGURE 2. A, size-exclusion chromatography for cAbBCII10 VHH, VHH_{ZnOBP1}, VHH_{ZnOBP2}, and VHH_{ZnOBP3}. Each 250- μ L sample was applied to a Superdex 75 10/300 GL column, and the absorbance of the eluant was monitored at a wavelength of 280 nm. B, circular dichroism spectra for the ZnOBP-grafted VHH fragments of cAbBCII10 VHH, VHH_{ZnOBP1}, VHH_{ZnOBP2}, and VHH_{ZnOBP3}.

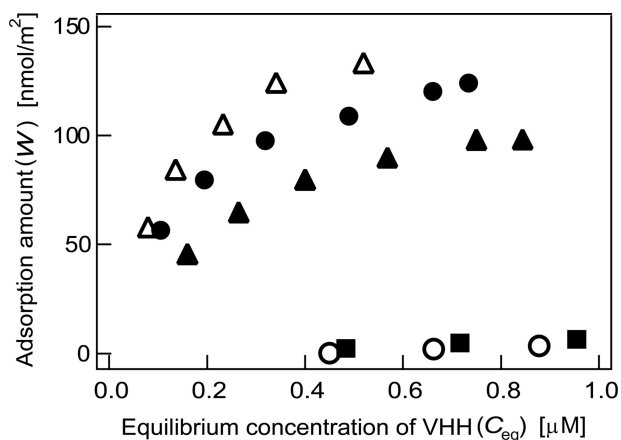


FIGURE 3. Adsorption isotherms for cAbBCII10 VHH (open circles), VHH_{ZnOBP1} (closed circles), VHH_{ZnOBP3} (closed squares), VHH_{ZnOBP1,3} (open triangles), and VHH_{ZnOBPtag} (closed triangles) against 0.2 mg of ZnO particles in 10 mM phosphate solution (pH 7.5; 200 mM NaCl, 0.05% Tween 20).

that most VHH fragments have a β -structure in the center region of CDR 2 (20, 29–31). This β -structure in CDR 2 might be important for scaffold stability. We therefore analyzed the binding affinity of VHH_{ZnOBP1} and VHH_{ZnOBP3} for the ZnO surface.

To measure the ability of ZnOBP-grafted VHH fragments to bind to the ZnO surface, we measured the adsorption isotherms of VHH_{ZnOBP1} and VHH_{ZnOBP3} for ZnO particles (Fig. 3). In a

phosphate solution, few cAbBCII10 VHH or VHH_{ZnOBP3} fragments were adsorbed onto ZnO particles, but, critically, VHH_{ZnOBP1} fragments were bound to ZnO particles with a dissociation equilibrium constant K_D comparable with that of VHH fragments with ZnOBP as a tag at the N terminus (VHH_{ZnOBP1}, 176 nM; VHH_{ZnOBPtag}, 303 nM; see Table 2): ZnOBP was as functional in CDR 1 as at the N terminus.

In addition, we grafted the ZnOBP sequence into CDR 3 of VHH_{ZnOBP1} (VHH_{ZnOBP1,3}) in an effort to improve the binding affinity for the ZnO surface; however, the K_D value of VHH_{ZnOBP1,3} was the same as that of VHH_{ZnOBP1} (Fig. 3 and Table 2). ZnOBP in the CDR 3 loop did not function effectively even in the presence of VHH_{ZnOBP1}.

Generation of High Affinity Antibody Fragments from Peptide-grafted VHH—To improve the binding affinity of ZnOBP-grafted VHH fragments, we employed a phage-display system whereby VHH_{ZnOBP1} with the CDR 3 loop randomized was displayed on the filamentous bacteriophage M13.

Evaluation of statistics on the frequency of amino acids in reported material-binding peptides selected from a phage display peptide library (5) revealed the preferential selection of Arg, His, and Lys residues among polar amino acids, and Thai *et al.* (32) have implied the presence of the Arg-Xaa-Xaa-Arg sequence in metal oxide binding. Here, we made a CDR 3 library with an $\alpha\beta\alpha$ -repeating sequence by utilizing degenerate codes; the β residues were randomized to Arg, Gly, Leu, or Val, and the α residues were randomized to Arg or His. Lys residues could not be included in the library because of the lack of flexibility of the codons encoding Lys.

Phages displaying VHH_{ZnOBP1} with CDR 3 randomized were mixed with ZnO particles, and unbound phages were removed by the addition of 10–50 mM phosphate solution containing 0.05% Tween 20. The residual phages bound to ZnO were separated from the ZnO particles by the addition of a 200 mM phosphate solution, because highly concentrated phosphate solution can inhibit protein adsorption. We examined the frequency of amino acid residues at each position in CDR 3 among the 200 clones randomly picked from the VHH_{ZnOBP1} library, before selection and after four rounds of selection (Fig. 4). His residues were dominantly selected at the α positions, and Leu and Gly residues were concentrated at the β positions (Fig. 4C). To estimate the binding affinities of selected clones, we chose four clones (3D2, 3E2, 4D4, and 4F2) and measured the adsorption isotherms of each VHH (Fig. 5). All the selected VHH fragments of each clone showed higher affinity for ZnO than did

TABLE 2

 Dissociation equilibrium constant (K_D) and maximum adsorption amount (W) of ZnOBP-grafted VHH fragments against ZnO

	K_D	W	Coefficient of determination ^a
	<i>nM</i>	<i>nmol/m²</i>	
cAbBCII10 VHH	ND ^b	ND	ND
VHH _{ZnOBP1}	176	152	0.999
VHH _{ZnOBP3}	ND	ND	ND
VHH _{ZnOBP1,3}	165	181	0.996
VHH _{ZnOBPtag}	303	142	0.995

^a Coefficient of determination is the square of correlation coefficients calculated from the fitting of Langmuir's adsorption isotherm by least square method. The value represents the degree of fitting coincidence.

^b ND means not detected.

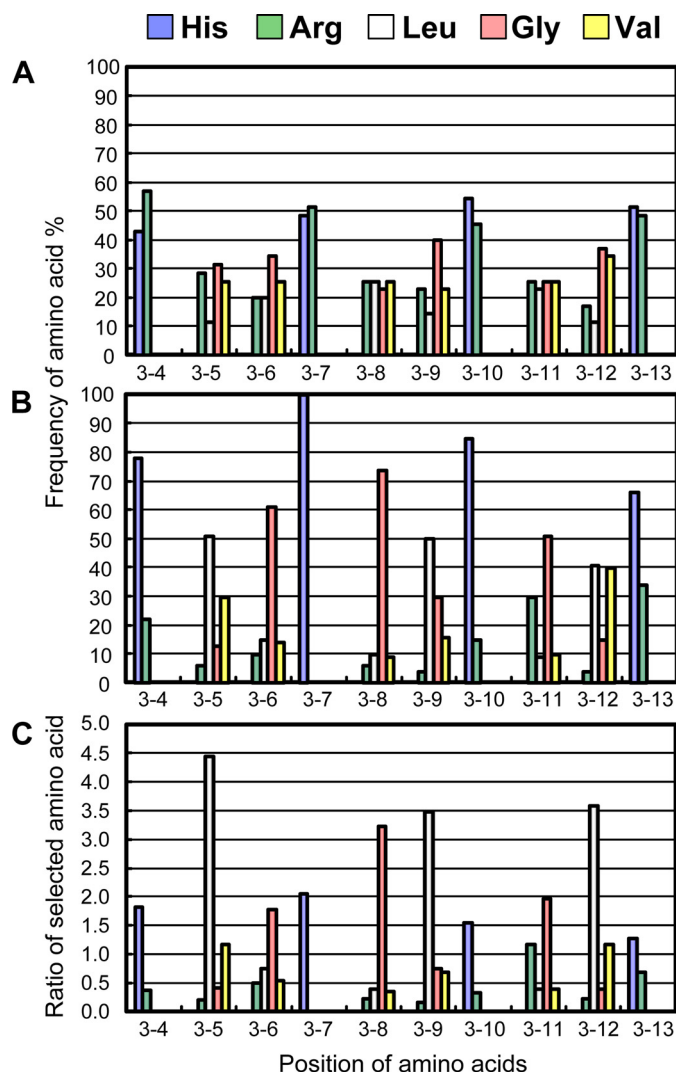


FIGURE 4. Frequencies of amino acids in randomized CDR 3 sequences of VHH_{ZnOBP1} before selection against ZnO (A) and after the fourth selection procedure with ZnO particles (B) are shown. The ratios of selected amino acids that are obtained by dividing the values in B by those in A are shown in C. Color bars are amino acids as follows: His (blue), Arg (green), Leu (white), Gly (red), and Val (yellow).

VHH_{ZnOBP1}; 4F2 VHH had a K_D value of 9 nM, about 20 times the affinity of VHH_{ZnOBP1} (Table 3). The binding affinity of VHH_{ZnOBP1} was thus improved by optimization of the CDR 3 sequence by molecular evolutionary methods.

Binding Properties of 4F2 VHH—To evaluate the role of selected CDR 3 sequence in 4F2 VHH (sZnOBP, HLGHGL-

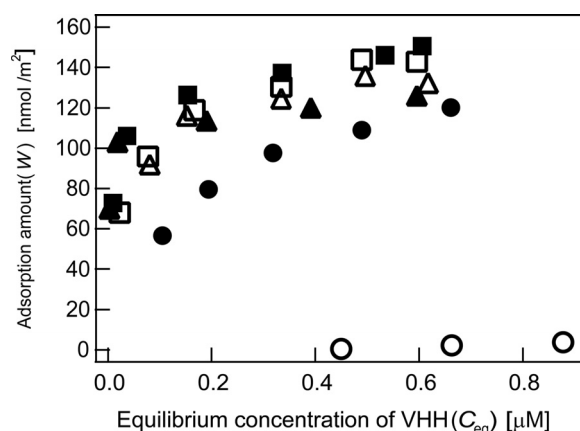


FIGURE 5. Adsorption isotherms for cAbBCII10 VHH (open circles), VHH_{ZnOBP1} (closed circles), 3D2 VHH (open triangles), 3E2 VHH (closed triangles), 4D4 VHH (open squares), and 4F2 VHH (closed squares) against 0.2 mg of ZnO particles in 10 mM phosphate solution (pH 7.5; 200 mM NaCl, 0.05% Tween 20).

TABLE 3

Selected VHH fragments after four rounds of selection against ZnO

Sequences selected by phage display methods are underlined. Amino acids of selected VHH are numbered as 3–1 to 3–16.

Fragment	Selected sequence in CDR3	K_D^a [nM]	W^b [nmol/m ²]	Coefficient of determination
	3–1			
3D2 VHH	VR <u>GH</u> LG <u>HGGHRLH</u> FRY	45	145	0.973
3E2 VHH	VR <u>GH</u> LG <u>HGGHGLH</u> FRY	21	119	0.982
4D4 VHH	VR <u>GHVGHGLHGV</u> FRY	25	141	0.966
4F2 VHH	VR <u>GH</u> LG <u>HGLHRVH</u> FRY	9	139	0.977

^a K_D is the equilibrium constant.

^b W is the maximum adsorption amount.

HRVH) for the binding onto the ZnO surface, we prepared the VHH fragment with CDR 1 of cAbBCII10 and CDR 3 of sZnOBP (VHH_{sZnOBP3}), and the binding affinity of VHH_{sZnOBP3} for ZnO was measured (supplemental Fig. S1A). The adsorption isotherm of VHH_{sZnOBP3} was adequately fitted by Langmuir adsorption isotherm equation, yielding a dissociation equilibrium constant K_D of 168 nM which is similar to that of VHH_{ZnOBP1} (supplemental Fig. S1B). Therefore, simultaneous binding of ZnOBP (EAHVMHKVAPRP) in CDR 1 and sZnOBP (HLGHGLHRVH) in CDR 3 is attributed to the high affinity of 4F2 VHH for the ZnO surface.

We further performed the competitive assay for the binding of VHH for ZnO surface by using the peptides of ZnOBP and sZnOBP (Fig. 6). In the competitive assay, VHH fragments were gradually dissociated from ZnO particles by increasing the concentration of the peptides in wash solution, and the dissociated VHH fragments were then analyzed by SDS-PAGE. In the mixture of ZnO particles and VHH_{ZnOBPtag}, the VHH fragments were dissociated from ZnO particles by the addition of ZnOBP and sZnOBP (Fig. 6A). Similar dissociation behavior of VHH was also observed for VHH_{ZnOBP1} and VHH_{sZnOBP3} (Fig. 6, B and C). These results imply that 4F2 VHH binds onto the ZnO surface with CDR 1 and 3 loops and, furthermore, that ZnOBP and sZnOBP bind onto identical local surface structure of ZnO. In the case of 4F2 VHH, few VHH fragments were dissociated from ZnO particles by adding the peptides of ZnOBP and

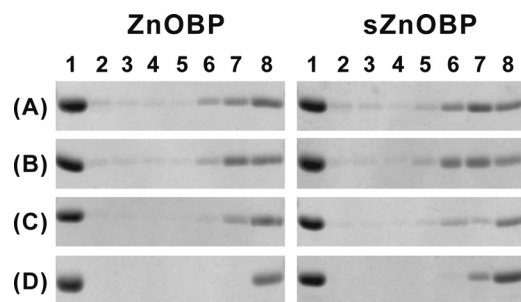


FIGURE 6. SDS-PAGE (18% acrylamide) results of competitive inhibition assay for the binding of VHH_{ZnOBPtag} (A), VHH_{ZnOBP1} (B), VHH_{sZnOBP3} (C), and 4F2 VHH for ZnO particles with the peptides of ZnOBP and sZnOBP (D). Lanes 1–8 correspond to added VHH solution, unadsorbed fraction, wash fraction, fractions eluted with 3, 30, and 300 μ M, and 3 mM peptide solutions, and fraction eluted with 6 M GdnHCl, respectively.

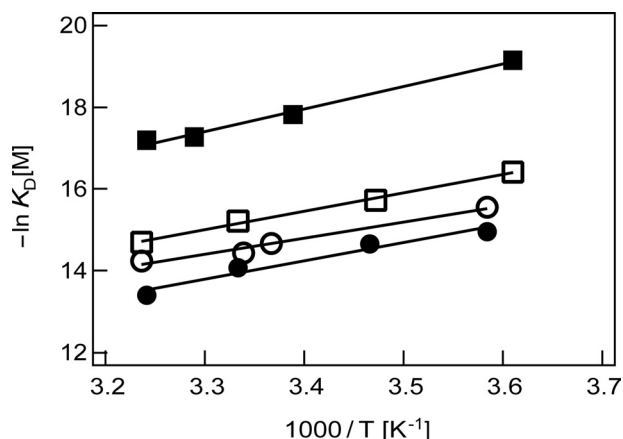


FIGURE 7. van't Hoff plot for the binding of VHH_{ZnOBPtag} (open circles), VHH_{ZnOBP1} (closed circles), VHH_{sZnOBP3} (open squares), and 4F2 VHH (closed squares) to ZnO. Straight lines were obtained by fitting the four points to the linearized van't Hoff equation as follows: $\ln K_D = \Delta H/RT - \Delta S/R$, where ΔH is van't Hoff enthalpy; ΔS is van't Hoff entropy, and R is universal gas constant.

sZnOBP at less than 3 mM that was 1000-fold of VHH concentration (Fig. 6D), which supports the results from adsorption isotherm measurement that 4F2 VHH have higher affinity for ZnO than VHH_{ZnOBP1} and VHH_{sZnOBP3}. It should be noted that the addition of 3 mM resulted in the dissociation of 4F2 VHH. These might indicate that the peptide of sZnOBP has higher affinity for ZnO than ZnOBP.

Thermodynamic Analysis of the Interaction between VHH and ZnO—To study the thermodynamics for the interaction of ZnO-binding VHH with ZnO surface, we measured the adsorption isotherm of VHH fragments for ZnO at various temperatures. The dissociation equilibrium constants K_D estimated from the adsorption isotherm at various temperatures were plotted to the van't Hoff representation ($\ln K_D = \Delta H/RT - \Delta S/R$) (Fig. 7). The series of K_D values showed a good correlation to the van't Hoff equation for all the VHH fragments, and enthalpies and entropies were obtained from the fitting (Table 4). It should be noted that all the ZnO-binding VHH fragments of VHH_{ZnOBP1}, VHH_{sZnOBP3}, and 4F2 VHH had large negative enthalpy changes for the binding to ZnO. This result suggests that the interactions of all the VHH fragments with ZnO surface is derived by enthalpy factor, i.e. electrostatic interaction. Furthermore, the fact that the evolution from VHH_{ZnOBP1} to

TABLE 4

Thermodynamic parameters of Gibbs free energy (ΔG), enthalpy (ΔH), and entropy (ΔS) of the binding of 4F2 VHH, VHH_{ZnOBP1}, VHH_{sZnOBP3}, VHH_{ZnOBPtag} for ZnO surface

The values were calculated from the K_D values by van't Hoff equation.

Fragment	ΔH	$T\Delta S$	$-\Delta G$
	<i>kJ/mol</i>	<i>kJ/mol</i>	<i>kJ/mol</i>
VHH _{ZnOBPtag}	-32.6	-3.6	36.2
VHH _{ZnOBP1}	-37.1	2.3	34.8
VHH _{sZnOBP3}	-37.3	-0.5	37.8
4F2 VHH	-45.7	-1.8	43.9

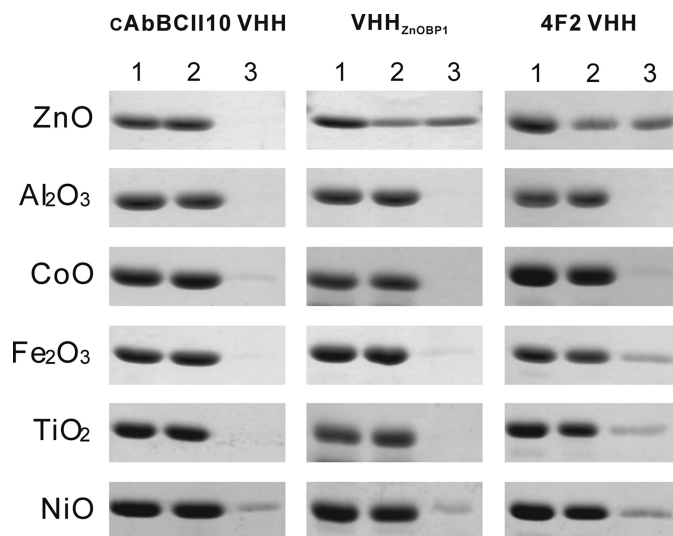


FIGURE 8. SDS-PAGE (18% acrylamide) analysis for the selectivity of VHH against ceramics. After the mixed solutions of each VHH (peptide-ungrafted VHH, VHH_{ZnOBP1}, or 4F2 VHH) and material particles (ZnO, Al₂O₃, CoO, Fe₂O₃, TiO₂, or NiO) had been centrifuged, the supernatant was removed, and the VHH adsorbed on the particles was eluted in 6 M GdnHCl solution. Lane 1, added VHH solution in particle suspension; lane 2, supernatant after centrifugation; lane 3, eluted fraction.

4F2 VHH increased the negative enthalpy change implies that the improvement of binding affinity is due to the increase of electrostatic interaction between VHH and ZnO surface.

Specificity of Anti-ZnO VHH Fragments for Other Ceramic Materials—To analyze the affinity of ZnO-binding VHH fragments for other materials, we mixed VHH fragments with particles of each material. After centrifugation, the supernatant was removed, and the VHH fragments adsorbed onto particles were separated by using a 6 M GdnHCl elute solution. Fig. 8 shows the SDS-PAGE results for the supernatant and elute solution. Few peptide-ungrafted VHH fragments were adsorbed onto any ceramic particles except NiO, whereas VHH_{ZnOBP1} bound to only ZnO and NiO particles. The finding that the amount of VHH_{ZnOBP1} adsorbed onto NiO was comparable with that of peptide-ungrafted VHH indicates that the framework structure of VHH was apt to be adsorbed onto the NiO particles. Therefore, VHH_{ZnOBP1} selectively bound to ZnO via the CDR 1 loop. In the case of 4F2 VHH, few VHH fragments were bound to CoO or Al₂O₃ particles, but some were adsorbed onto Fe₂O₃ and TiO₂. However, the K_D values of 4F2 VHH for Fe₂O₃ and TiO₂ were 745 and 286 nM, respectively, indicating much lower binding affinity than for ZnO (Table 3). Therefore, the high binding ability of 4F2 VHH to ceramic materials is ZnO-specific.

High Affinity Anti-inorganic Material Antibody Generation

TABLE 5

Selected VHH fragments after four rounds of selection against Al₂O₃ and CoO

Sequences selected by phage display methods are underlined. Numbering of the amino acids of VHH_{Al₂O₃} and VHH_{CoOBP1} follows the Kabat numbering system (20). Amino acids of selected VHH are numbered as 3–1 to 3–16.

Fragment	Selected sequence in CDR 3	K_D^a [nM]	W^b [nmol/m ²]	Coefficient of determination
Against Al ₂ O ₃ :				
VHH _{Al₂O₃}	95 <u>VRGYFMRLPSSHNFRY</u> 102	3100	180	0.990
4C5 VHH	3-1 <u>VRGHLRHGLHLRHFRY</u> 3-16	49	115	0.990
4D7 VHH	<u>VRGHLGHGVHLRHFRY</u>	220	112	0.999
4E1 VHH	<u>VRGHLRHGLHGVFRY</u>	55	111	0.998
4G1 VHH	<u>VRGHVGRGGHGLFRY</u>	53	127	0.997
Against CoO:				
VHH _{CoOBP1}	95 <u>VRGYFMRLPSSHNFRY</u> 102	1080	102	0.995
4B3 VHH	3-1 <u>VRGHVVHGGHGVFRY</u> 3-16	140	301	0.976
4E3 VHH	<u>VRGHLGHVRLHFRY</u>	124	426	0.991
4H1 VHH	<u>VRGRVVHGGHGVFRY</u>	219	299	0.990
4H12 VHH	<u>VRGRVVHGGHGVFRY</u>	— ^c	— ^c	— ^c

^a K_D is equilibrium constant.

^b W is maximum adsorption amount.

^c The amounts of 4H12 VHH fragments prepared by *E. coli* expression were too small to measure adsorption isotherms.

Availability of the Construction Method of Material-binding Antibodies for Other Inorganic Materials—We attempted to generate anti-Al₂O₃ VHH fragments from a reported Al₂O₃-binding peptide (KRHKQKTSRMGK) (23) and anti-CoO VHH fragments from a reported CoO-binding peptide (LGKDRPHF-HRS) (24). Grafting of the peptide into the CDR 1 loop functionalized the VHH fragments. Although the peptide grafting into CDR 3 showed no functionalization, the evolutionary approach in CDR 3 critically increased the affinity for the corresponding material surface (Table 5). VHH fragments with high affinity for gold have also been generated; hence, the construction of antibody by integrating grafting and evolution technology, we call CANIGET, can widely generate high affinity antibodies against inorganic material surfaces.

We examined the specificities of anti-Al₂O₃ 4G1 and anti-CoO 4E3 VHH fragments for various materials (Fig. 9). Unlike the case with VHH_{ZnOBP1}, VHH_{Al₂O₃} with Al₂O₃-binding peptide and VHH_{CoOBP1} with CoO-binding peptide in CDR 1 did not show clear specificity for each ceramic material, because of the broad material specificity of the peptides used. The finding that both the 4G1 and 4E3 VHH fragments had ambiguous material specificities implies that the material specificity of high affinity antibodies generated by construction of antibody by integrating grafting and evolution technology is strongly dependent on the characteristics of the grafted peptide.

Application of 4F2 VHH to Bio-interface Molecule—To utilize 4F2 VHH for spontaneous selective protein immobilization on a ZnO plate in a flow system, we developed a solution con-

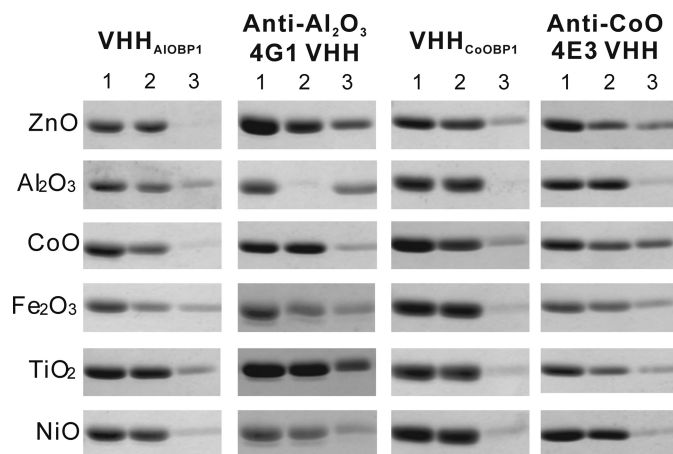


FIGURE 9. SDS-PAGE (18% acrylamide) analysis of the selectivity of VHH_{Al₂O₃}, anti-Al₂O₃ 4G1 VHH, VHH_{CoOBP1}, and anti-CoO 4E3 VHH against ZnO, Al₂O₃, CoO, Fe₂O₃, TiO₂, and NiO. After the solutions of VHH and material particles were centrifuged, the supernatant was removed, and the VHH adsorbed onto the particles was eluted with 6 M GdnHCl solution. Lane 1, VHH solution added to particle suspension; lane 2, supernatant after centrifugation; lane 3, eluted fraction.

taining anti-ZnO VHH fragments on a ZnO film deposited on a silicon plate and detected immobilization of the protein by reflectometric interference spectroscopy (Fig. 10A). Under flow conditions, the time-dependent change in wavelength with minimum intensity in the reflected spectrum showed little adsorption of peptide-ungrafted VHH fragments on the ZnO film, whereas definite spontaneous immobilization of VHH_{ZnOBP1}, VHH_{ZnOBPtag}, and 4F2 VHH was observed, with the amounts of adsorbed protein comparable with those estimated under batch conditions (Tables 2 and 3). It should be noted that the dissociation of 4F2 VHH was too slow to be observed in the dissociation process.

Fig. 10B shows stepwise protein immobilization on ZnO film via bispecific VHH dimer. Bispecific VHH dimers were constructed by fusing anti-GFP VHH to the C terminus of 4F2 VHH via a hinge linker. The VHH dimers bound the surface of ZnO film with the same binding strength as 4F2 VHH, and then GFP loaded after injection of the VHH dimers was immobilized on the ZnO film. When we estimated the binding activity of each VHH domain in the bispecific dimer from the amounts of immobilized protein in Fig. 10B, the 4F2 VHH and anti-GFP VHH domains in the dimer retained 100 and 81% of their activity on the ZnO film; seven GFP proteins were immobilized on a 100-nm² area. The conservation of the activity of both VHH domains and the high rates of occupancy of the ZnO film by GFP indicate that the bispecific VHH dimer format with the high affinity material-binding antibody fragment was effective as a bio-interface molecule for direct and easy immobilization of proteins.

DISCUSSION

Single Domain Camel VHH Fragment as a Framework for Grafting Material-binding Peptide—The structural resemblance of human and mouse Fv frameworks enables the transfer of binding function to humanized antibodies (33); these replacement techniques are currently applied to the design of new functional antibody fragments by the grafting of alien

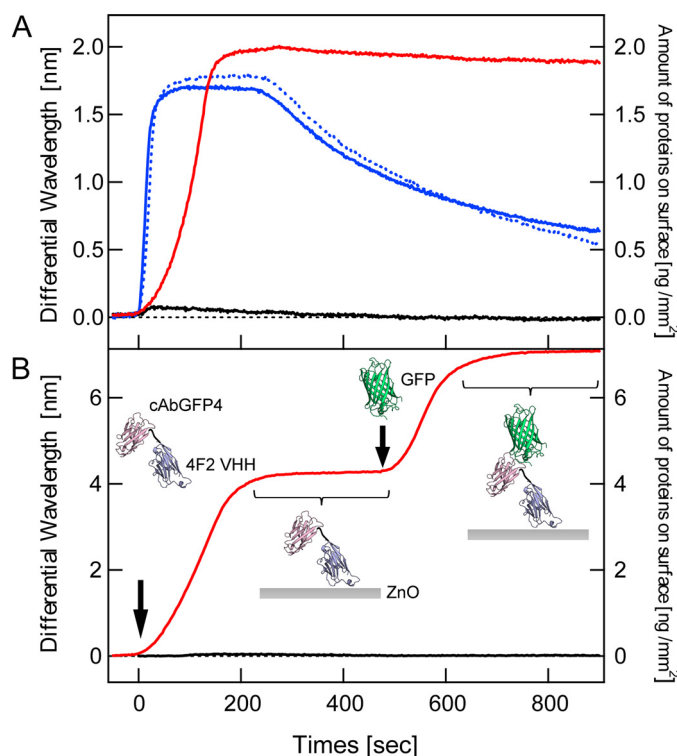


FIGURE 10. **Spontaneous stepwise-stacking of proteins on ZnO via 4F2 VHH.** A, reflectometric interference sensorgrams for interaction of 4F2 VHH (red, solid line), VHH_{ZnOBP1} (blue, solid line), VHH_{ZnOBP1tag} (blue, dotted line), and cAbBCII10 VHH (black, solid line) with ZnO film. Each VHH solution (1 μM) was injected for 240 s. B, reflectometric interference sensorgram (red, solid line) of the interaction of bispecific VHH dimers with ZnO film and GFP. VHH dimer solution (1 μM) was injected for 240 s, after which time GFP proteins were injected. Arrow indicates the timing of GFP injection. Black line corresponds to the sensorgram measured when only GFP proteins were injected for 240 s.

motif peptide sequences (34–36). Previously, we functionalized an Fv fragment from mouse anti-lysozyme antibody HyHEL-10 by grafting material-binding peptides into the heavy chain CDR 2 region (22); however, the replacement caused dissociation of the Fv fragment. The framework used did not have enough structural versatility for the grafting of material-binding peptide sequences.

Here, we used the variable fragment from a camel antibody, cAbBCII10 VHH, as a new framework for the grafting of material-binding peptide. The cAbBCII10 VHH fragment is a single domain with a framework tolerant to various CDR loop structures (20). cAbBCII10 VHH was also an appropriate stable framework for the replacement of CDRs 1 and 3 with material-binding peptides, although grafting into the CDR 3 loop did not functionalize VHH. Our previous study of the Fv fragment suggested the importance of the exposure of grafted material-binding peptide by means of a scaffold (22); however, the CDR 1 and 3 loops are sufficiently exposed in the reported crystal structure of cAbBCII10 VHH (31). The general VHH fragment recognizes an antigen by using the CDR 1 and 3 loops (37); in particular, CDR 3 has a greater variety of length and conformation than other CDRs, and the variety generates a single-domain VHH equal in binding affinity to heterodimer Fv. The length and conformational variety of CDR 3 are accompanied by the interaction of CDR 3 with frameworks and CDR 1, which con-

trols the orientation of CDR 3 to give high binding affinity (38). In this study, our grafting design for CDR 3 might have yielded an improper conformation of ZnOBP, *i.e.* grafting into CDR 3 might have required more careful design. Our results demonstrate that CDR 3 should be functionalized by molecular evolution rather than by peptide grafting.

Affinity Maturation of ZBP-grafted VHH by Molecular Evolution in CDR 3—There have been a few studies of the selection of antibodies with affinity for material surfaces by using general methodologies with *in vivo* immune systems (15) or *in vitro* library methods (16–19). However, because of the low immunogenic potential of solid materials, far fewer antibodies with affinities for material surfaces have been selected than those with affinities for soluble molecules. Even with the use of *in vitro* selection methods, the limited library diversity and strong nonspecific interactions of coat proteins on phages with solid bulk surfaces make it difficult to select positive antibodies. We demonstrated here the possibility of steadily generating high affinity antibodies by coupling the grafting of peptides from a reported material-binding peptide repertoire and molecular evolution of the peptide-grafted variable fragment. The construction of a library from a low affinity antibody for which the binding site could be predicted allowed us to narrow down the segments that needed to be randomized, thus enabling us to bypass the limitations of library diversity.

Randomization of the CDR 3 loop in the format of the $\alpha\beta\beta\alpha$ repeating sequence can also decrease the necessary magnitude of library diversity. The $\alpha\beta\beta\alpha$ format was designed in consideration of the Arg-Xaa-Xaa-Arg format (32), the importance of His residues for inorganic material binding (39), and the frequent appearance of Arg, His, and Lys residues in material-binding peptides. Use of the $\alpha\beta\beta\alpha$ format with Arg/Gly/Leu/Val at the β positions and His/Arg at the α positions resulted in the preferential selection of Gly/Leu (β) and His (α) in the selection of VHH against ZnO. Notably, few Arg residues were selected at both the β and α positions. These results suggest that in CDR 3 in the VHH scaffold, Arg has less functional ability than His to bind to the ZnO surface.

Synergistic Effect of CDR Loops on Binding on the ZnO Surface—In this study, we focused the binding properties of the highest affinity 4F2 VHH fragment. The comparison with VHH_{ZnOBP1} and VHH_{sZnOBP3} indicates that the high binding affinity of 4F2 VHH resulted from synergistic effect from grafted CDR 1 and selected CDR 3 loops in the VHH framework (Fig. 6). The competitive binding assay by using the peptides of ZnOBP and sZnOBP implied that CDR 1 and CDR 3 recognized identical local surface structure of ZnO.

To increase the affinity of the peptides with micromolar K_D values, repetition and clustering of material-binding peptides are among the possible approaches to increasing the binding affinity of peptides that have micromolar K_D values (3). One polypeptide with three repeats of a gold-binding peptide had a K_D value of 89 nM (40), and clustering of 24 titania-binding peptides on a ferritin protein increased the binding affinity, giving a K_D value of 11 nM (41). Our high affinity antibody fragments showed strong binding with only two loop structures (CDRs 1 and 3). Therefore, use of the antibody format has the

High Affinity Anti-inorganic Material Antibody Generation

potential for efficient generation of high affinity interface molecules from material-binding peptides.

Thermodynamic Analysis for the Binding of Anti-ZnO VHH to ZnO Surface—The thermodynamic parameters estimated from van't Hoff plots demonstrated dominant change of enthalpy in the absorption process of all the ZnO-binding VHH fragments (VHH_{ZnOBPtag}, VHH_{ZnOBP1}, VHH_{sZnOBP3}, and 4F2 VHH) on the ZnO surface. This result is comparable with the binding properties of anti-gold antibody Fv fragment, A14P-b2 Fv (18). This implies that coulombic interaction dominates the binding process of anti-ZnO VHH fragments on ZnO. Considering that ZnO surface and the framework of VHH are positively charged at the pH value of 7.5, the grafted and selected CDR loops electrostatically interact with the ZnO surface. In general, one of major factors for protein adsorption on material surface is entropy changes that result from dehydration of the absorbent surface and from the conformational change of adsorbed proteins (42, 43). Therefore, our thermodynamic result implies that the conformation of anti-ZnO VHH fragments is little changed by interaction with the ZnO surface and that few water molecules on ZnO surface are dispersed by the binding of VHH. When the CD spectra were measured on 4F2 VHH fragments with ZnO nanoparticles, we observed the CD spectra derived from the immunoglobulin structure of camel antibody (data not shown). Hence, 4F2 VHH was not denatured on the ZnO surface.

Application of High Affinity Antibody Fragment for Nanobiotechnology—Antibody fragments are among the smallest units with naturally occurring binding domains, and an advantage of using them as high affinity interface molecules is the fact that various fusion technologies can be used. Artificial antibody formats constructed for therapeutic and imaging uses have been used to generate multivalent and multispecific material-binding antibodies to functionalize nanoparticles and to spontaneously and selectively accumulate proteins and nanoparticles on patterned spots on substrate (18, 44). Here, we show the potential of high affinity material-binding antibodies for selective immobilization of proteins on biosensor plates. The fusion of material-binding peptides and antibody fragments enables direct and oriented protein immobilization without the need for complicated processes (9, 45), and unmodified inorganic surfaces can directly receive electrons from immobilized redox proteins without mediators (46). Improving the binding strength of material-binding biomolecules will lead to more quantitative and reliable detection.

In conclusion, we generated antibody fragments with high affinity for inorganic material surfaces from low affinity material-binding peptides by the integration of peptide-grafting and phage-display techniques. The scaffold of the single-domain VHH fragment was so stable that VHH was directly functionalized by grafting of the material-binding peptide into CDR 1 without structural destabilization. Application of the $\alpha\beta\alpha$ motif library to the CDR 3 of peptide-grafted VHH enabled us to bypass limitations on library diversity; consequently, this construction method allow us to generate high affinity antibodies against material surfaces from previously identified material-binding peptides. Quantitative thermodynamic analysis described the enthalpy synergistic effect from grafted and

selected CDR loops in VHH, which shows the potential of antibody scaffold for creating high affinity small interface units with efficient binding mechanism. Use of the high affinity antibody fragments resulted in stable selective protein immobilization on material surfaces in flow systems. We expect to be able to use such material-binding antibodies as biointerface units for nanoscale quantitative biosensing and protein accumulation.

REFERENCES

1. Carvalho, A. L., Goyal, A., Prates, J. A., Bolam, D. N., Gilbert, H. J., Pires, V. M., Ferreira, L. M., Planas, A., Romão, M. J., and Fontes, C. M. (2004) *J. Biol. Chem.* **279**, 34785–34793
2. Itoh, Y., Kawase, T., Nikaidou, N., Fukada, H., Mitsutomi, M., Watanabe, T., and Itoh, Y. (2002) *Biosci. Biotechnol. Biochem.* **66**, 1084–1092
3. Brown, S. (1997) *Nat. Biotechnol.* **15**, 269–272
4. Whaley, S. R., English, D. S., Hu, E. L., Barbara, P. F., and Belcher, A. M. (2000) *Nature* **405**, 665–668
5. Sarikaya, M., Tamerler, C., Jen, A. K., Schulten, K., and Baneyx, F. (2003) *Nat. Mater.* **2**, 577–585
6. Mao, C., Solis, D. J., Reiss, B. D., Kottmann, S. T., Sweeney, R. Y., Hayhurst, A., Georgiou, G., Iverson, B., and Belcher, A. M. (2004) *Science* **303**, 213–217
7. Naik, R. R., Stringer, S. J., Agarwal, G., Jones, S. E., and Stone, M. O. (2002) *Nat. Mater.* **1**, 169–172
8. Tamerler, C., Duman, M., Oren, E. E., Gungormus, M., Xiong, X., Kacar, T., Parviz, B. A., and Sarikaya, M. (2006) *Small* **2**, 1372–1378
9. Park, T. J., Lee, S. Y., Lee, S. J., Park, J. P., Yang, K. S., Lee, K. B., Ko, S., Park, J. B., Kim, T., Kim, S. K., Shin, Y. B., Chung, B. H., Ku, S. J., Kim do, H., and Choi, I. S. (2006) *Anal. Chem.* **78**, 7197–7205
10. Brown, S. (2001) *Nano Lett.* **1**, 391–394
11. Umetsu, M., Mizuta, M., Tsumoto, K., Ohara, S., Takami, S., Watanabe, H., Kumagai, I., and Adschiri, T. (2005) *Adv. Mater.* **17**, 2571–2575
12. Kramer, R. M., Li, C., Carter, D. C., Stone, M. O., and Naik, R. R. (2004) *J. Am. Chem. Soc.* **126**, 13282–13286
13. Adams, G. P., and Weiner, L. M. (2005) *Nat. Biotechnol.* **23**, 1147–1157
14. Kessler, N., Perl-Treves, D., and Addadi, L. (1996) *FASEB J.* **10**, 1435–1442
15. Geva, M., Frolow, F., Eisenstein, M., and Addadi, L. (2003) *J. Am. Chem. Soc.* **125**, 696–704
16. Barbas, C. F., 3rd, Rosenblum, J. S., and Lerner, R. A. (1993) *Proc. Natl. Acad. Sci. U.S.A.* **90**, 6385–6389
17. Artzy Schirman, A., Zahavi, E., Yeager, H., Rosenfeld, R., Benhar, I., Reiter, Y., and Sivan, U. (2006) *Nano Lett.* **6**, 1870–1874
18. Watanabe, H., Nakanishi, T., Umetsu, M., and Kumagai, I. (2008) *J. Biol. Chem.* **283**, 36031–36038
19. Watanabe, H., Tsumoto, K., Taguchi, S., Yamashita, K., Doi, Y., Nishimiya, Y., Kondo, H., Umetsu, M., and Kumagai, I. (2007) *Bioconjug. Chem.* **18**, 645–651
20. Saerens, D., Pellis, M., Loris, R., Pardon, E., Dumoulin, M., Matagne, A., Wyns, L., Muyldermans, S., and Conrath, K. (2005) *J. Mol. Biol.* **352**, 597–607
21. Sato, K., Tsuchiya, M., Saldanha, J., Koishihara, Y., Ohsugi, Y., Kishimoto, T., and Bendig, M. M. (1994) *Mol. Immunol.* **31**, 371–381
22. Hattori, T., Umetsu, M., Nakanishi, T., Tsumoto, K., Ohara, S., Abe, H., Naito, M., Asano, R., Adschiri, T., and Kumagai, I. (2008) *Biochem. Biophys. Res. Commun.* **365**, 751–757
23. Krauland, E. M., Peelle, B. R., Wittrup, K. D., and Belcher, A. M. (2007) *Biotechnol. Bioeng.* **97**, 1009–1020
24. Schembri, M. A., Kjaergaard, K., and Klemm, P. (1999) *FEMS Microbiol. Lett.* **170**, 363–371
25. Maenaka, K., Furuta, M., Tsumoto, K., Watanabe, K., Ueda, Y., and Kumagai, I. (1996) *Biochem. Biophys. Res. Commun.* **218**, 682–687
26. Brunauer, S., Emmett, P. H., and Teller, E. (1938) *J. Am. Chem. Soc.* **60**, 309–319
27. Rothbauer, U., Zolghadr, K., Tillib, S., Nowak, D., Schermelleh, L., Gahl, A., Backmann, N., Conrath, K., Muyldermans, S., Cardoso, M. C., and Leonhardt, H. (2006) *Nat. Methods* **3**, 887–889
28. Conrath, K. E., Lauwereys, M., Galleni, M., Matagne, A., Frère, J. M.,

- Kinne, J., Wyns, L., and Muyldermans, S. (2001) *Antimicrob. Agents. Chemother.* **45**, 2807–2812
29. Decanniere, K., Desmyter, A., Lauwereys, M., Ghahroudi, M. A., Muyldermans, S., and Wyns, L. (1999) *Structure* **7**, 361–370
30. Conrath, K., Vincke, C., Stijlemans, B., Schymkowitz, J., Decanniere, K., Wyns, L., Muyldermans, S., and Loris, R. (2005) *J. Mol. Biol.* **350**, 112–125
31. Vincke, C., Loris, R., Saerens, D., Martinez-Rodriguez, S., Muyldermans, S., and Conrath, K. (2009) *J. Biol. Chem.* **284**, 3273–3284
32. Thai, C. K., Dai, H., Sastry, M. S., Sarikaya, M., Schwartz, D. T., and Baneyx, F. (2004) *Biotechnol. Bioeng.* **87**, 129–137
33. Jones, P. T., Dear, P. H., Foote, J., Neuberger, M. S., and Winter, G. (1986) *Nature* **321**, 522–525
34. Barbas, C. F., 3rd, Languino, L. R., and Smith, J. W. (1993) *Proc. Natl. Acad. Sci. U.S.A.* **90**, 10003–10007
35. Moroncini, G., Kanu, N., Solforosi, L., Abalos, G., Telling, G. C., Head, M., Ironside, J., Brookes, J. P., Burton, D. R., and Williamson, R. A. (2004) *Proc. Natl. Acad. Sci. U.S.A.* **101**, 10404–10409
36. Frederickson, S., Renshaw, M. W., Lin, B., Smith, L. M., Calveley, P., Springhorn, J. P., Johnson, K., Wang, Y., Su, X., Shen, Y., and Bowdish, K. S. (2006) *Proc. Natl. Acad. Sci. U.S.A.* **103**, 14307–14312
37. Muyldermans, S. (2001) *J. Biotechnol.* **74**, 277–302
38. Muyldermans, S., and Lauwereys, M. (1999) *J. Mol. Recognit.* **12**, 131–140
39. Peelle, B. R., Krauland, E. M., Wittrup, K. D., and Belcher, A. M. (2005) *Langmuir* **21**, 6929–6933
40. Tamerler, C., Oren, E. E., Duman, M., Venkatasubramanian, E., and Sarikaya, M. (2006) *Langmuir* **22**, 7712–7718
41. Sano, K., Ajima, K., Iwahori, K., Yudasaka, M., Iijima, S., Yamashita, I., and Shiba, K. (2005) *Small* **1**, 826–832
42. Norde, W., and Lyklema, J. (1978) *J. Colloid Interface Sci.* **66**, 257–265
43. Norde, W., and Lyklema, J. (1979) *J. Colloid Interface Sci.* **71**, 350–366
44. Umetsu, M., Hattori, T., Kikuchi, S., Muto, I., Nakanishi, T., Watanabe, H., and Kumagai, I. (2008) *J. Mater. Sci.* **23**, 3241–3246
45. Woodbury, R. G., Wendin, C., Clendenning, J., Melendez, J., Elkind, J., Bartholomew, D., Brown, S., and Furlong, C. E. (1998) *Biosens. Bioelectron.* **13**, 1117–1126
46. Habermüller, K., Mosbach, M., and Schuhmann, W. (2000) *Fresenius J. Anal. Chem.* **366**, 560–568